Electron transfer in voltage tunable two-color infrared photodetectors

Amlan Majumdar[a)]
Department of Electrical Engineering, Princeton University, Princeton, New Jersey 08544

K. K. Choi
U. S. Army Research Laboratory, Adelphi, Maryland 20783

L. P. Rokhinson
Department of Electrical Engineering, Princeton University, Princeton, New Jersey 08544

J. L. Reno
Sandia National Laboratories, Albuquerque, New Mexico 87185

D. C. Tsui
Department of Electrical Engineering, Princeton University, Princeton, New Jersey 08544

(Received 8 October 2001; accepted for publication 7 January 2002)

Two-color quantum-well infrared photodetectors (QWIPs) that are based on electron transfer between coupled QWs suffer from the presence of the shorter wavelength peak at all bias voltages. We investigate this problem in such detectors with 50 or 200 Å AlGaAs barriers between the QW pair. We deduce the absorption coefficient α and photoconductive gain g of the detectors with 50 Å barriers using corrugated QWIPs with different corrugation periods. We find that α has a number of small peaks in its spectrum but its value remains almost constant between 0.1 and 0.2 μm^{-1} in the 6–12 μm range for most experimental conditions. The wavelength dependence of g, which always has a pronounced peak at the shorter detection wavelength, determines the responsivity line shape. These results are attributed to insufficient electron transfer between the coupled QWs and to low tunneling probability of the longer wavelength photoelectrons. A comparison of measured responsivity and calculated absorption spectrum of the detectors with 200 Å barriers indicates that there is significant electron transfer between the coupled wells. Despite efficient electron transfer, these detectors have a shorter wavelength detection peak at all bias voltages because of significant short wavelength absorption in both the QWs. © *2002 American Institute of Physics*.
[DOI: 10.1063/1.1455684]

I. INTRODUCTION

Two-color photodetection has many important applications such as remote temperature sensing, chemical analysis, and target identification and discrimination.[1,2] For remote temperature sensing, the peak detection wavelength of the detector must switch from one wavelength to another when a variable, such as bias voltage, is changed. Two-color quantum-well infrared photodetectors (QWIPs) are suitable for this purpose because their peak absorption wavelength and spectral bandwidth can be tailored by varying device and material parameters such as QW width, barrier composition, and barrier thickness. The simplest two-color QWIPs are three-terminal devices with two stacks of multiple QWs (MQWs).[3,4] In these detectors, each MQW stack, sandwiched between two heavily doped contact layers, is designed to detect a different wavelength. In detector array applications, such as infrared cameras, each QWIP acts as a pixel. In order to obtain separate optical signal from each detector, it is necessary to keep the middle contact common, and the top and bottom contacts as independent pixel contacts. Focal plane arrays with this contact scheme have serious problems in detector readout electronics.[5]

Voltage tunable two-color QWIPs that have one MQW stack between two contact layers are two-terminal devices where the peak detection wavelength can be changed by a bias voltage. These detectors when used with time-multiplexed readout circuits immensely simplify the fabrication of focal plane arrays. Voltage tunable two-color detectors have been proposed in the past based on Stark shift or electron transfer between coupled QWs under an applied bias. The first approach relies on the shift of energy levels under an applied electric field. For MQW structures that contain square QWs, this shift is small since first-order linear shift is forbidden by symmetry. Large Stark shifts have been observed in asymmetric MQW structures with coupled QWs[6] or graded barriers[7,8] or asymmetric step wells.[9,10]

The second approach is based on transfer of electrons between ground states of coupled QWs under an applied bias V_b. The electron transfer process was first observed in MQW structures that had alternately doped QWs.[11] It was later used to demonstrate a voltage tunable two-color modulator[12] and detector.[13] In these QWIPs, the peak detection wavelength can be changed by reversing the polarity of V_b. Unfortunately, the shorter wavelength peak is always present for both bias polarities. This makes voltage switching less effective for longer wavelength detection.

[a)]Author to whom correspondence should be addressed; electronic mail: majumdar@ee.princeton.edu

 © 2002 American Institute of Physics

Downloaded 01 Apr 2002 to 128.112.49.85. Redistribution subject to AIP license or copyright, see http://ojps.aip.org/japo/japcr.jsp

We investigated the origin of this problem in a QWIP structure where each period had a pair of QWs coupled through a 50 Å AlGaAs barrier.[14] This detector, designed for 8.2 and 10.7 μm detection, had a V_b independent detection peak at 8 μm but a voltage tunable cutoff wavelength. The absence of the longer wavelength responsivity peak for $V_b < 0$ V could be due to negligible absorption or low gain. For a better understanding, we extracted absorption coefficient α and photoconductive gain g at 6 and -6 V bias voltages at temperature $T=10$ K using corrugated QWIPs (CQWIPs) with different corrugation periods.[15–17] Our results at 10 K indicated insufficient electron transfer between the coupled QWs and low tunneling probability of the longer wavelength photoelectrons. In this article, we report on the complete characterization of this detector in the bias range from -6 to 6 V for temperatures ranging from 10 to 70 K. We also report on the fabrication of a detector with a 200 Å thick AlGaAs barrier between the QW pair and show that electron transfer is significantly enhanced in this detector.

This article is organized as follows. We describe the first QWIP structure and the electron transfer based photodetection mechanism in Sec. II, show responsivity data of CQWIPs in Sec. III, and present the deduced spectra of α and g in Sec. IV. In Sec. V, we design a new detector, show its measured responsivity and calculated absorption spectra, and demonstrate efficient electron transfer between the coupled QWs. We summarize the main results in Sec. VI.

II. DETECTOR STRUCTURE

We use two different two-color QWIP structures for the experiments described in this article. The first two-color QWIP, referred to as wafer structure A, consists of 36 periods of coupled QWs sandwiched between a 0.5 μm thick n^+-GaAs top contact layer (1×10^{18} cm^{-3} Si doping) and a 1.5 μm thick n^+-GaAs bottom contact layer (5×10^{17} cm^{-3} Si doping). Each period consists of a 40 Å GaAs well coupled to a 44 Å GaAs well through a 50 Å $Al_{0.28}Ga_{0.72}As$ barrier and separated from the next set of coupled wells by a 200 Å $Al_{0.28}Ga_{0.72}As$/300 Å $Al_{0.22}Ga_{0.78}As$ step barrier. All the wells are uniformly doped (5×10^{17} cm^{-3} Si doping) and the barriers undoped. The entire structure is grown on a semi-insulating GaAs substrate by molecular beam epitaxy (MBE). We will describe the second detector structure in Sec. V because its design is based on the results obtained from wafer A in Sec. IV.

At zero bias, the 40 Å wide left QW (LQW) has two bound states separated by 116 meV ($\lambda=10.7$ μm) while the 44 Å wide right QW (RQW) has a bound state and an extended state with an energy difference of 151 meV ($\lambda=8.2$ μm). The conduction band diagram of this detector under an applied bias is shown in Figs. 1(a)–1(b). We apply V_b to the top contact while keeping the bottom one grounded. For positive bias, electrons are transferred from the ground state of the LQW to the ground state of the RQW by tunneling. When infrared radiation is coupled into this detector, electrons are photoexcited from the ground state of the RQW to the extended state above it. These photoelectrons are swept away by the electric field to produce a photocurrent. Thus, we expect to detect 8.2 μm radiation for positive bias. For negative bias, electrons tunnel from the ground state of the RQW to that of the LQW and should allow the detection of 10.7 μm radiation. It is important to note that for negative bias, these longer wavelength (lower energy) photoelectrons have to tunnel through a triangular barrier before contributing to photocurrent.

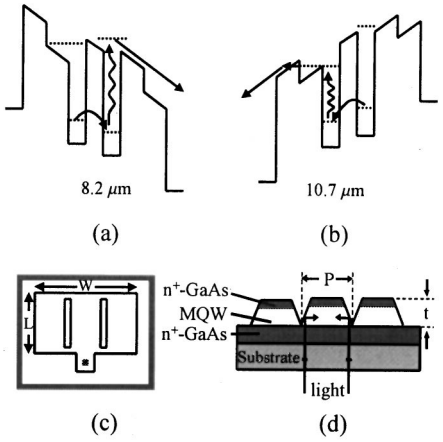

FIG. 1. Conduction band diagram and photodetection mechanism of two-color QWIP based on coupled QWs for (a) positive and (b) negative bias V_b. The peak detection wavelengths are for wafer A. (c) Top view and (d) cross-sectional view of a CQWIP with three corrugations. All the CQWIPs are $L=700$ μm long and $W=1200$ μm wide and have a 150×150 μm^2 top contact pad.

III. PARAMETER EXTRACTION

A. CQWIP processing

We processed a set of eight CQWIPs from wafer A with corrugation period $P=10$, 15, 20, 30, 40, 60, 300, and 1200 μm for extracting α and g. The CQWIP structure is defined by photolithography and wet etching. The top and cross-sectional views of a CQWIP with three corrugations is shown in Figs. 1(c)–1(d). t is the thickness of the top contact layer and active MQW layers that are etched away. Each CQWIP is 1200 μm wide and 700 μm long and has a 150×150 μm^2 top contact pad. Au/Ge/Au (200/200/1500 Å) contacts were evaporated and then alloyed at 420 °C for 5 s to form ohmic contacts to the top and bottom n^+-GaAs layers. Subsequently, the detector substrate was thinned down to about 200 μm and then polished. As shown in Fig. 1(d), back illuminated normal incidence infrared light undergoes total internal reflection at the etched sidewalls to get coupled to the intersubband transitions in the MQWs.

B. CQWIP model

The CQWIP model used for extracting α and g is described in great detail in Ref. 17. Measured responsivity R is converted into normalized responsivity (NR) using $NR(P)=R(P)/r_d(P)$, where r_d is the ratio of the 77 K dark currents of a CQWIP with period P and a CQWIP with no corrugations ($P=1200$ μm in our case). We fit the following expression to our data:[17]

Downloaded 01 Apr 2002 to 128.112.49.85. Redistribution subject to AIP license or copyright, see http://ojps.aip.org/japo/japcr.jsp

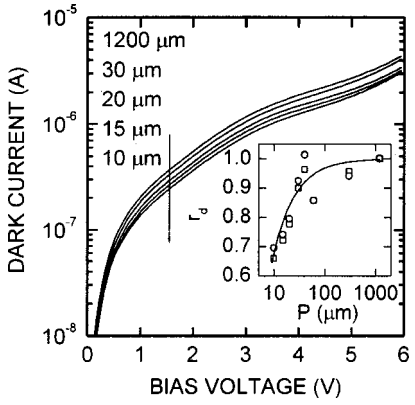

FIG. 2. Dark current I_d vs bias V_b of CQWIPs from wafer A at 77 K for $V_b>0$ V. The five curves are for CQWIPs with period $P=1200$, 30, 20, 15, and 10 μm (top to bottom curve). (Inset) Dark current ratio r_d vs P at 77 K, symbols: experimental data at $V_b=2$ (squares) and -2 V (circles), and line: $r_d=(P-t)/P$, with $t=2.8$ μm.

$$NR(P)=\frac{R(P)}{r_d(P)}=\frac{e}{h\nu}g\frac{1}{P-t}\left(t+\frac{e^{-\alpha P}}{2\alpha}(1-e^{2\alpha t})\right)+R_0\frac{P}{P-t}, \quad (1)$$

where $h\nu$ is the energy of infrared radiation and R_0 is CQWIP responsivity when P is very large. α, g, and R_0 are fitting parameters and $t=2.8$ μm is the etch depth for the CQWIPs.

Variations in the amount of active detector material arising from processing nonuniformities are eliminated by using *NR* instead of *R*. These nonuniformities arise from small differences in slit width of photoresist or etching depth in different parts of the wafer. For the same nominal *P*, a detector with a smaller amount of active material will have a smaller dark current I_d and a smaller photocurrent $I_{\rm ph}$. By using $NR(P)=R(P)/r_d(P)\propto I_{\rm ph}(P)/I_d(P)$, we compensate all processing nonuniformities because r_d is used for estimating the amount of active material left in a CQWIP after wet etching. For this method to work, wafer growth has to be uniform such that the current density is the same across the wafer. We measured 77 K dark current of 200×200 μm^2 mesas processed from different parts of wafer A and found them to be within 1% of each other. This demonstrates that the MBE-grown wafer is extremely uniform.

C. CQWIP dark current

The 77 K dark current I_d of a few CQWIPs is shown in Fig. 2 for positive bias. The detector with a larger P has a larger I_d because it has more active material. The dark current ratio $r_d=I_d(P)/I_d(P=1200$ μm) is shown in the inset of Fig. 2 as a function of P for $V_b=2$ and -2 V with symbols. In the absence of processing nonuniformities, $r_d=(P-t)/P$ for 45° etched sidewalls. Here t is the etch depth of the CQWIPs. This value of r_d, which is assumed in the derivation of Eq. (1), is shown in the inset of Fig. 2 with a line for $t=2.8$ μm. The deviation of the data (symbols) from the line indicates that material variations do exist in our CQWIPs. It also justifies the use of *NR* instead of *R* for parameter extraction.

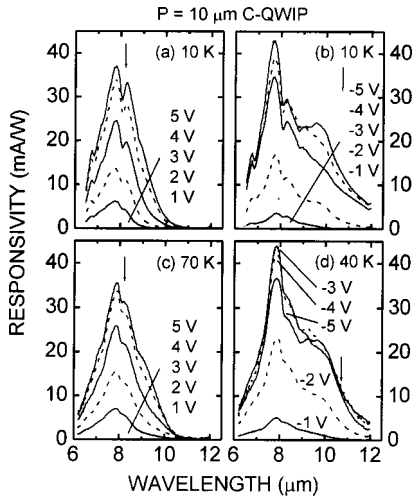

FIG. 3. Spectral responsivity R of CQWIP with period $P=10$ μm fabricated from wafer A for: (a) $V_b>0$ V and 10 K, (b) $V_b<0$ V and 10 K, (c) $V_b>0$ V and 70 K, and (d) $V_b<0$ V and 40 K. The arrows indicate the calculated peak positions of the strongest intersubband transitions ($\lambda=8.2$ μm for $V_b>0$ V and $\lambda=10.7$ μm for $V_b<0$ V) assuming complete electron transfer between the coupled wells under an applied bias.

D. CQWIP photoresponse

Spectral responsivity R was measured for all the CQWIPs with different corrugation periods at $T=10$, 40, and 70 K using standard ac lock-in techniques. The highest temperature at which R could be measured reliably is 70 K for positive bias and 40 K for negative bias. At temperatures higher than these, the large dark current flowing through the detector overloads the input stage of the lock-in amplifier. We show responsivity spectra of the $P=10$ μm CQWIP in Fig. 3. For positive bias, the peak detection wavelength is 7.8 μm at both 10 and 70 K. In addition to the 7.8 μm responsivity peak, there are two small peaks at 6.8 and 8.2 μm at 10 K and only a shoulder at 8.2 μm at 70 K. For negative bias, the main responsivity peak is at 7.8 μm for both 10 and 40 K. Apart from the 7.8 μm peak, there are two small peaks at 6.8 and 8.2 μm at 10 K. There is also a shoulder around 9.8 μm for $-4\leqslant V_b<0$ V that develops into a fourth peak at -5 V. At 40 K, the 6.8 and 8.2 μm peaks are not resolved while the shoulder around 9.8 μm at small negative bias becomes a well resolved peak at -5 V.

The line shape of the responsivity spectra of all the CQWIPs is similar to that of the $P=10$ μm CQWIP. We convert the responsivity data to *NR* using $NR=R/r_d$. Figure 4(a) depicts typical *NR* spectra of CQWIPs with different corrugation period P at -3 V and 10 K. The largest *NR* is for the $P=10$ μm CQWIP and the smallest for the $P=1200$ μm one. *NR* decreases with P as expected because the average optical intensity in a corrugation decreases with increasing P. From Fig. 4(a), we obtain the value of *NR* at a fixed wavelength for different values of P. The results at -3 V and 10 K are plotted in Figs. 4(b)–4(c) for different wavelengths. We fit Eq. (1) to this data and obtain α, g, and R_0. The

Downloaded 01 Apr 2002 to 128.112.49.85. Redistribution subject to AIP license or copyright, see http://ojps.aip.org/japo/japcr.jsp

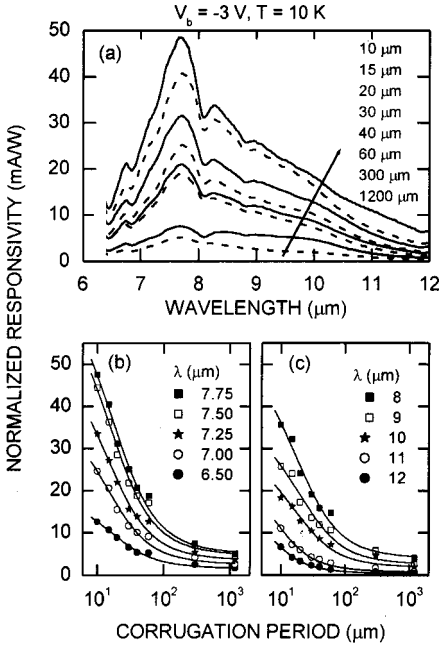

FIG. 4. *NR* of CQWIPs from wafer A at −3 V and 10 K. (a) *NR* spectra for corrugation period $P=10$, 15, 20, 30, 40, 60, 300, and 1200 μm (top to bottom curve). (b)–(c) *NR* vs *P* at different wavelengths: (symbols) experimental data from (a) and (lines) least-squares fit of Eq. (1) to the data.

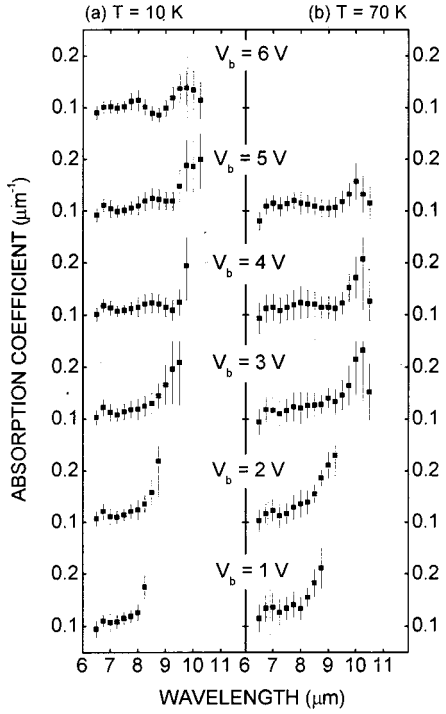

FIG. 5. Absorption coefficient spectra of structure A at: (a) 10 K and (b) 70 K for different positive bias voltages. α is extracted from fitting Eq. (1) to normalized responsivity data.

least-squares fit is shown with lines and we see that Eq. (1) fits the data well. We repeated this fitting procedure for different operating conditions and obtained fits as good as the ones shown in Figs. 4(b)–4(c). This indicates that the CQWIP model, which was originally proposed for one-color QWIPs, describes infrared absorption in two-color QWIPs satisfactorily. The deduced parameters α, g, and R_0 are presented in Sec. IV.

IV. DETECTOR PARAMETERS

A. Absorption coefficient α

The absorption coefficient α obtained from the extraction procedure is plotted for different positive bias voltages in Fig. 5. At 10 K, α has a small peak at 6.8 μm and increases with λ for $\lambda > 7$ μm and $V_b \leqslant 3$ V. At $V_b = 4$ and 5 V, there are two small peaks at 6.8 and 8.5 μm, while at $V_b = 6$ V there are three small peaks at 6.8, 8, and 9.8 μm. At 70 K, we observe α has a small peak around 7 μm for all values of V_b, a larger peak around 10 μm for $V_b \geqslant 3$ V, and a very small peak around 8 μm for $V_b \geqslant 4$ V. The deduced spectra of α under negative bias are shown in Fig. 6. There is a small absorption peak at 6.8 μm for all negative voltages. For $|V_b| \leqslant 4$ V, α has a second broad peak around 8.5 μm. For $|V_b| \geqslant 5$ V, this 8.5 μm peak disappears while another peak emerges at 10 μm. This 10 μm peak has a large long-wavelength tail. At 40 K, there is an absorption peak around 6.8 μm, a second peak around 8 μm for $|V_b| \geqslant 2$ V, and a third peak at higher wavelengths around 10.5 μm for $|V_b| \geqslant 3$ V.

Figures 5 and 6 show a number of small peaks in the spectrum of α. The value of α lies between 0.1 and 0.2 μm^{-1} for most values of V_b and T. Within the limits of error of the parameter extraction procedure, there is insignificant change in α as a function of V_b at the same T. This result is different from that observed by Choi *et al.*[17] and Liu *et al.*[18] for one-color QWIPs. Using the same parameter extraction scheme used in this work, Choi *et al.*[17] observed up to 26%

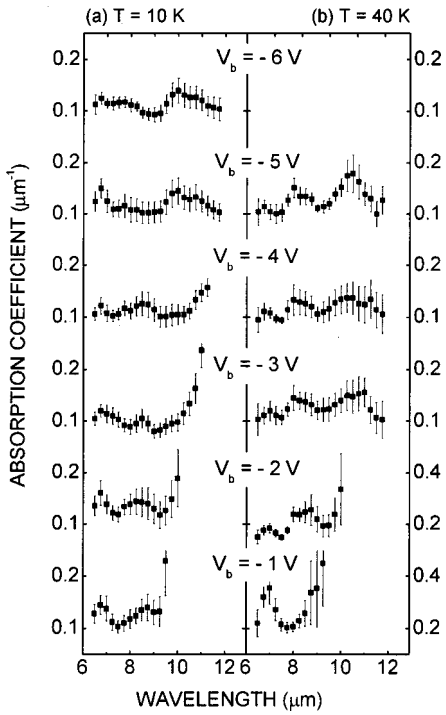

FIG. 6. Absorption coefficient spectra of structure A at: (a) 10 K and (b) 40 K for different negative bias voltages. α is extracted from fitting Eq. (1) to normalized responsivity data.

Downloaded 01 Apr 2002 to 128.112.49.85. Redistribution subject to AIP license or copyright, see http://ojps.aip.org/japo/japcr.jsp

reduction of α as V_b was increased from 1 to 5 V for a QWIP with a peak detection wavelength of 8.4 μm. For a 9 μm QWIP, Liu *et al.*[18] found an 11% reduction in absorbance as V_b was increased from 0 to 5 V. Both groups attributed their results to the depletion of electrons in the QWs under an applied bias. Our results, therefore, indicate that the total number of electrons in the QW pair does not change with bias in the -6 to 6 V range.

Figures 5 and 6 also show, within the limits of error, that α practically does not change with T at the same V_b except for the 6.8 μm peak at $V_b=-1$ V. For an 8.4 μm QWIP, Choi *et al.*[17] found a 14% reduction of α as T was decreased from 70 to 10 K. Their observation was explained by finite carrier freezeout at low temperatures. The lack of any T dependence of α in the 10–70 K range in our QWIP, therefore, implies insignificant carrier freezeout.

If there is significant electron transfer between the coupled QWs under an applied bias, the absorption spectrum $\alpha(\lambda)$ should exhibit distinct peaks around 8.2 and 10.7 μm for positive and negative bias, respectively. For most operating conditions, $\alpha \approx 0.1-0.2\ \mu\text{m}^{-1}$ is approximately constant in the 6–12 μm wavelength range. Also, there are small peaks in α at both short ($\lambda \approx 8$ μm) and long ($\lambda \approx 10$ μm) wavelengths for both bias polarities. This suggests insufficient transfer of electrons between the coupled QWs under an applied bias. We ascribe this to the small voltage drop between the coupled QWs. The coupled wells have a 50 Å AlGaAs barrier between them and are separated from the next set of coupled wells by a 500 Å AlGaAs step barrier. Voltage division between these two barriers leads to less than 10% of the voltage drop across each period of the MQW to drop between the coupled QWs. For example, at $V_b=6$ V, only 15 mV drops across the 50 Å barrier between the coupled wells out of the 160 mV that drops across each period of the MQW.

B. Photoconductive gain *g*

The deduced values of detector gain g are plotted in Fig. 7 for different operating conditions. g has a very pronounced peak at 7.8 μm for both bias polarities in the temperature range 10–70 K. For positive bias, g decreases sharply for $\lambda > 7.8$ μm and is zero for $\lambda > 10$ μm. However, for negative bias, g decreases slowly beyond 7.8 μm and does not go to zero for long wavelengths. There is a distinct shoulder around 9.5 μm that becomes a small peak at -5 V and 40 K (not shown in Fig. 7). It is also clear from Fig. 7 that for $V_b>0$ V, g increases almost linearly with V_b up to 5 V at 10 K and 4 V at 70 K and then saturates. For $V_b<0$ V, g increases sharply with increasing $|V_b|$ up to -3 V at both 10 and 40 K and saturates at higher negative voltages. The pronounced peak in gain at 7.8 μm and the relatively wavelength insensitive α lead to the bias independent 8 μm peak detection wavelength. From Figs. 3 and 7, we see that the line shape of R is determined by the line shape of g. The peak value of g (≈ 0.03) implies that photoelectrons from one QW, on the average, travel just one period in the MQW structure before being captured by another QW.

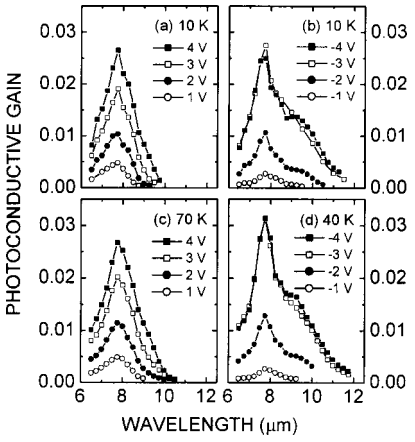

FIG. 7. Photoconductive gain spectra of structure A for: (a) $V_b>0$ V and 10 K, (b) $V_b<0$ V and 10 K, (c) $V_b>0$ V and 70 K, and (d) $V_b<0$ V and 40 K. The lines are a guide to the eye. g is extracted from fitting Eq. (1) to normalized responsivity data. Typical error bars are 10% and have been omitted from the graphs for clarity.

The presence of the 7.8 μm peak in gain for all biases and the lack of any peak in g around 10.7 μm for negative bias can be explained as follows. The 7.8 μm peak corresponds to the bound-to-continuum transition in the RQW, whereas the peak at 10.7 μm, which is absent for $V_b<0$ V, is from the bound-to-bound transition in the LQW [see Figs. 1(a)–1(b)]. Once photoexcited, the short wavelength electrons are swept away by the electric field while the long wavelength photoelectrons have to tunnel through a triangular barrier before being swept away by the electric field to form a photocurrent. Therefore, the gain of the short wavelength photoelectrons is much larger than that of the long wavelength ones. Consequently, there is a 7.8 μm peak in gain at all voltages and no peak around 10.7 μm for negative bias.

C. R_0

The third detector parameter R_0, which accounts for the experimentally observed nonzero responsivity of CQWIPs with very large P, is shown in Fig. 8 for $T=10$ K. The 40 and 70 K R_0 spectra have similar peak positions and line shape. From Figs. 3 and 8, it is clear that R_0 and R have the same peak positions and similar linewidth at the same V_b and

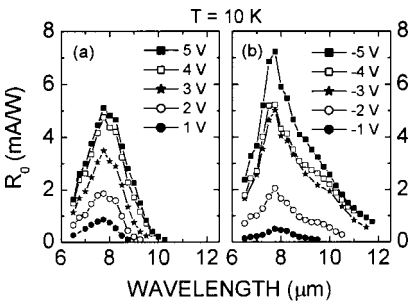

FIG. 8. Spectrum of R_0 of structure A at 10 K for: (a) $V_b>0$ V and (b) $V_b<0$ V. The lines are a guide to the eye. R_0 is extracted from fitting Eq. (1) to normalized responsivity data. Typical error bars are 5% and have been omitted from the graphs for clarity.

Downloaded 01 Apr 2002 to 128.112.49.85. Redistribution subject to AIP license or copyright, see http://ojps.aip.org/japo/japcr.jsp

T and very similar bias dependence at all temperatures. These observations, similar to that of Chen *et al.*[16] and Choi *et al.*,[17] indicate that R_0 arises from the same intersubband transitions in the MQW that lead to R. R_0 is attributed to the responsivity from the p-polarized light reflected from the two mesa edges that are perpendicular to the corrugations.

V. ENHANCED ELECTRON TRANSFER BETWEEN COUPLED QWs

In the previous section, we found that detector A has the following problems: (i) insufficient electron transfer between the coupled QWs under an applied bias, and (ii) low tunneling probability, and hence, low gain of the longer wavelength photoelectrons. To enhance electron transfer, a larger potential difference is needed between the coupled wells. This can be achieved by growing a thicker AlGaAs barrier between the QW pair. The tunneling probability and photoconductive gain of the longer wavelength photoelectrons can be increased if a thinner $Al_{0.28}Ga_{0.72}As$ layer is used in the step barrier between the adjacent periods in the MQW. We designed and fabricated a new detector based on these considerations.

A. Structure

The new QWIP structure, grown on a semi-insulating GaAs substrate by MBE and referred to as wafer structure B, consists of 36 periods of coupled QWs sandwiched between top (0.5 μm thick, 1×10^{18} cm^{-3} Si doping) and bottom (1.5 μm thick, 5×10^{17} cm^{-3} Si doping) n^+-GaAs contact layers. Each period consists of a 40 and a 44 Å GaAs QW coupled through a 200 Å $Al_{0.28}Ga_{0.72}As$ barrier. The thickness of this barrier was increased from 50 Å in structure A to enhance electron transfer between the QW pairs. The QW pairs are separated from each other by a 50 Å $Al_{0.28}Ga_{0.72}As$/300 Å $Al_{0.22}Ga_{0.78}As$ step barrier. The $Al_{0.28}Ga_{0.72}As$ part of this step barrier was decreased from 200 Å in wafer A to increase the gain of the longer wavelength photoelectrons. The 40 Å LQWs are uniformly doped (7×10^{17} cm^{-3} Si doping) while the 44 Å RQWs and the barriers are undoped. Only the LQWs are doped to ensure the depletion of the RQWs for longer wavelength detection at negative bias. For positive bias, electrons transfer from the LQW to the RQW and lead to the detection of the shorter wavelength radiation.

B. Responsivity

We processed 45°-edge coupled QWIPs from wafer B for detector characterization. 200×200 μm^2 mesas were defined by photolithography and wet etching. A 1500 Å thick layer of AuGe alloy was evaporated and then alloyed at 420 °C for 5 s to form ohmic contacts to the top and bottom n^+-GaAs layers. 45° edges were then polished on the sides of the samples to couple infrared radiation to the intersubband transitions in the MQWs.

The responsivity of these 45° edge coupled detectors was measured at 10 K in the 6–12 μm wavelength range. The responsivity spectrum of a typical detector is depicted in Fig. 9. For positive bias up to 3 V, there is a pronounced peak at 8 μm and small peaks at 6.4, 7.3, and 10.3 μm. At V_b $=4$ V, the 7.3 and 10.3 μm peaks are not resolved in R although there is a shoulder at 7 μm. For small negative bias up to -1 V, there are two broad peaks centered at 8.2 and 9.7 μm and a small peak at 6.3 μm. At higher negative bias, the 8.2 μm peak develops into two peaks. One of these peaks shifts down to 7.9 μm and its position is independent of the bias voltage. The other peak shifts to higher wavelengths with increasing bias and is centered at 8.7 μm for -3 V. The second broad peak at 9.7 μm for -1 V also shifts to higher wavelengths with increasing V_b and is at 10.5 μm for -3 V. The small peak at 6.3 μm is independent of V_b for $-4 \leqslant V_b \leqslant -1$ V.

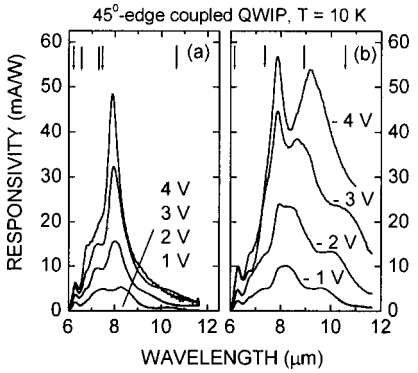

FIG. 9. Spectral responsivity R of 45°-edge coupled QWIP from wafer B measured at 10 K for: (a) $V_b>0$ V and (b) $V_b<0$ V. In both (a) and (b), $|V_b|=1$, 2, 3, and 4 V from the bottom to the top curve. The arrows indicate the calculated peak positions at: (a) $V_b=3$ V and (b) $V_b=-3$ V assuming complete electron transfer between the QW pair.

C. Calculated absorption spectrum

We calculated the energy levels and wave functions of structure B for different values of V_b using the transfer matrix method.[1] At zero bias, the lowest levels E_1 and E_2 are 2 meV apart with E_1 in the RQW and E_2 in the LQW. Both the wells are occupied. The Fermi energy E_F is 6 meV for the two-dimensional electron density $n_{2D}=2.8\times10^{11}$ cm^{-2} in each unit of the MQW. For positive bias, the separation between E_1 and E_2 increases. When the energy difference exceeds 10 meV, all the electrons should be in the RQW with $E_F=10$ meV. This is the case at $V_b=3$ V where E_2 is 30 meV above E_1. For negative bias, E_1 is in the LQW and its separation from E_2 in the RQW increases with $|V_b|$. At V_b $=-3$ V, E_1 is 25 meV below E_2. Thus, all the electrons should be in the LQW with $E_F=10$ meV.

The oscillator strength of optical transitions from the ground state of each QW to the excited states is obtained from the computed wave functions. Then we calculated the absorption spectrum under the assumption that there is complete electron transfer under an applied bias and that each individual transition is inhomogeneously broadened. Random fluctuations in material parameters like the well width and the barrier height cause inhomogeneous broadening of intersubband transitions.[19] The broadened line shape considered here is Gaussian. A standard deviation of 8 meV was found to give the best fits to the peak positions in responsiv-

Downloaded 01 Apr 2002 to 128.112.49.85. Redistribution subject to AIP license or copyright, see http://ojps.aip.org/japo/japcr.jsp

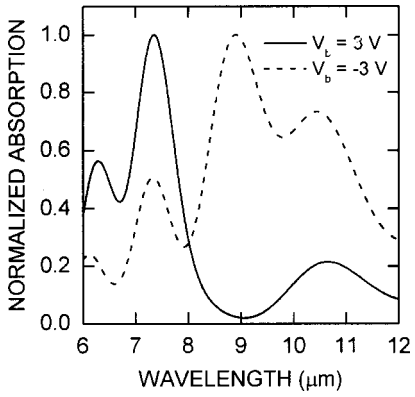

FIG. 10. Calculated absorption spectrum of structure B at bias voltage $V_b = 3$ and -3 V assuming complete electron transfer between the QW pair.

ity. The calculated absorption spectra $\alpha(\lambda)$ are shown in Fig. 10 for $V_b = 3$ and -3 V.

D. Discussion

If there is complete transfer of electrons between the QWs under an applied bias, the peak positions in the responsivity spectrum $R(\lambda)$ should match the peak positions of $\alpha(\lambda)$. The relative sizes of the responsivity peaks need not be the same as that of $\alpha(\lambda)$ because responsivity depends on both $\alpha(\lambda)$ and energy dependent photoconductive gain g. At $V_b = 3$ V, there are three peaks in $\alpha(\lambda)$ at 6.3, 7.3, and 10.6 μm. The 6.3 μm peak is a combined result of $E_1 \rightarrow E_{11}$ and $E_1 \rightarrow E_{12}$ transitions. Since E_1 is in the RQW, we call the $E_1 \rightarrow E_{11}$ transition R11. The 7.3 μm peak comes from the combined R9 and R10 transitions while the 10.6 μm peak is from the R6 transition. These three peak positions are in excellent agreement with the observed $R(\lambda)$ peaks at 6.3, 7.3, and 10.3 μm. The fourth responsivity peak at 8 μm is, however, not seen in calculated $\alpha(\lambda)$. It is most likely due to the shifted R9 transition in the actual growth structure. At $V_b = -3$ V, $\alpha(\lambda)$ has four peaks at 6.1, 7.3, 8.9, and 10.5 μm due to L13, L10, L7, and L6 transitions, respectively. These peak positions match well with the peaks in $R(\lambda)$ at 6.3, 7.9, 8.7, and 10.5 μm. Based on this good agreement between the peak positions of measured $R(\lambda)$ and calculated $\alpha(\lambda)$, we conclude that there is significant electron transfer between the QW pair.

Despite the efficient electron transfer, the short wavelength peak is present in detector B at all voltages. There are a number of excited states in the detector for both positive and negative bias. From Fig. 10, we observe that the short wavelength absorption peak is inherent to this detector structure. The 7.3 μm peak in $\alpha(\lambda)$ is only two thirds the size of the 10.1 μm peak and half the size of the 8.9 μm peak. Therefore, even after complete electron transfer between the coupled QWs, the short wavelength peak is present in the responsivity spectrum for both bias polarities. Thus, despite efficient electron transfer at negative bias, the similar oscillator strength of transitions from the ground state in the LQW to the excited states for both short and long wavelengths continues to limit the wavelength tunability of this detector design. Further improvement would require wave function engineering to reduce α at shorter wavelengths for negative bias voltages.

VI. CONCLUSION

In conclusion, we have investigated the presence of the shorter wavelength peak for both bias polarities in a two-color QWIP that is based on transfer of electrons between coupled QWs under a bias. We fabricated detectors with 50 or 200 Å AlGaAs barriers between the coupled wells. The first structure, with 50 Å barriers, exhibits a bias independent peak detection wavelength at 8 μm but a voltage tunable cutoff wavelength. We used CQWIPs with different corrugation periods to extract α and g in the bias range from -6 to 6 V and temperature range 10–70 K. We found a number of small peaks in the spectrum of α. However, the value of α is between 0.1 and 0.2 μm^{-1} in the 6–12 μm range for most values of V_b and T that indicated insufficient electron transfer between the coupled QWs. We also found a pronounced peak in g at the shorter wavelength for all values of V_b and T. The absence of a longer wavelength peak in g for negative bias is attributed to the low tunneling probability of the longer wavelength photoelectrons. Based on these results, we concluded that a thicker AlGaAs barrier between the QW pair should enhance electron transfer. We therefore fabricated the second detector with 200 Å thick AlGaAs barriers and observed significant electron transfer between the QW pairs. Despite efficient electron transfer, the shorter wavelength peak is always present in the second detector due to significant short wavelength absorption in both quantum wells.

ACKNOWLEDGMENT

The work at Princeton University is supported by the Army Research Office and the National Science Foundation. Sandia is a multiprogram laboratory operated be Sandia Corporation, a Lockheed Martin Company, for the United States Department of Energy under Contract No. DE-AC04-94AL85000.

[1] K. K. Choi, *The Physics of Quantum Well Infrared Photodetectors* (World Scientific, River Edge, NJ, 1997).
[2] C. J. Chen, K. K. Choi, W. H. Chang, and D. C. Tsui, Appl. Phys. Lett. **72**, 7 (1998).
[3] A. Kock, E. Gornik, G. Abstreiter, G. Bohm, M. Walther, and G. Weimann, Appl. Phys. Lett. **60**, 2011 (1992).
[4] I. Grave, A. Shakouri, N. Kuze, and A. Yariv, Appl. Phys. Lett. **60**, 2362 (1992).
[5] S. D. Gunapala *et al.*, IEEE Trans. Electron Devices **47**, 963 (2000); M. Sundaram *et al.*, Infrared Phys. Technol. **42**, 301 (2001).
[6] K. K. Choi, B. F. Levine, C. G. Bethea, J. Walker, and R. J. Malik, Phys. Rev. B **39**, 8029 (1989).
[7] S. R. Parihar, S. A. Lyon, M. Santos, and M. Shayegan, Appl. Phys. Lett. **55**, 2417 (1989).
[8] B. F. Levine, C. G. Bethea, B. O. Shen, and R. J. Malik, Appl. Phys. Lett. **57**, 383 (1990).
[9] E. Martinet, F. Luc, E. Rosencher, P. Bois, and S. Delaitre, Appl. Phys. Lett. **60**, 895 (1992).
[10] E. Martinet, E. Rosencher, F. Luc, P. Bois, E. Costard, and S. Delaitre, Appl. Phys. Lett. **61**, 246 (1992).
[11] K. K. Choi, B. F. Levine, C. G. Bethea, J. Walker, and R. J. Malik, Appl. Phys. Lett. **52**, 1979 (1988).

Downloaded 01 Apr 2002 to 128.112.49.85. Redistribution subject to AIP license or copyright, see http://ojps.aip.org/japo/japcr.jsp

[12] N. Vodjdani, B. Vinter, V. Berger, E. Bockenhoff, and E. Costard, Appl. Phys. Lett. **59**, 555 (1991).
[13] V. Berger, N. Vodjdani, P. Bois, B. Vinter, and S. Delaitre, Appl. Phys. Lett. **61**, 1898 (1992).
[14] A. Majumdar, K. K. Choi, L. P. Rokhinson, and D. C. Tsui, Appl. Phys. Lett. **80**, 538 (2002).
[15] C. J. Chen, K. K. Choi, M. Z. Tidrow, and D. C. Tsui, Appl. Phys. Lett. **68**, 1446 (1996).
[16] C. J. Chen, K. K. Choi, L. Rokhinson, W. K. Chang, and D. C. Tsui, Appl. Phys. Lett. **75**, 3210 (1999).
[17] K. K. Choi, C. J. Chen, and D. C. Tsui, J. Appl. Phys. **88**, 1612 (2000).
[18] H. C. Liu, M. Buchanan, Z. R. Wasilewski, and H. Chu, Appl. Phys. Lett. **58**, 1059 (1992).
[19] K. K. Choi, S. V. Bandara, S. D. Gunapala, W. K. Liu, and J. M. Fastenau, J. Appl. Phys. **91**, 551 (2002).

Downloaded 01 Apr 2002 to 128.112.49.85. Redistribution subject to AIP license or copyright, see http://ojps.aip.org/japo/japcr.jsp